Quantitative evaluation of transient valence orbital occupations in a 3d transition metal complex as seen from the metal and ligand perspective

Raphael M. Jay[a], Sebastian Eckert[a,1], Rolf Mitzner[b], Mattis Fondell[b] and Alexander Föhlisch[a,b]

[a]Institut für Physik und Astronomie, Universität Potsdam, Karl-Liebknecht-Straße 24/25, 14476 Potsdam, Germany.
[b]Institute for Methods and Instrumentation for Synchrotron Radiation Research, Helmholtz-Zentrum Berlin für Materialien und Energie GmbH, Albert-Einstein-Straße 15, 12489 Berlin, Germany.

ARTICLE INFO

Keywords:
Iron cyanides, photochemistry, soft X-ray absorption

ABSTRACT

It is demonstrated for the case of photo-excited ferrocyanide how time-resolved soft X-ray absorption spectroscopy in transmission geometry at the ligand K-edge and metal L_3-edge provides quantitatively equivalent valence electronic structure information, where signatures of photo-oxidation are assessed locally at the metal as well as the ligand. This allows for a direct and independent quantification of the number of photo-oxidized molecules at two soft X-ray absorption edges highlighting the sensitivity of X-ray absorption spectroscopy to the valence orbital occupation of 3d transition metal complexes throughout the soft X-ray range.

1. Introduction

Changes in oxidation state are common steps during photo-chemical reactions involving transition metal complexes. For an unambiguous characterization of the involved transient species, it is therefore crucial to spectroscopically follow the underlying changes in orbital population. The photo-oxidation of aqueous ferrocyanide ($[Fe(CN)_6]^{4-}$) constitutes an ideal model process that allows to test the capabilities of different spectroscopies in that regard. After an optical excitation in the ultraviolet regime, a Fe 3d electron is ejected into the solvent [1]. Thereby, the Fe(II) complex $[Fe(CN)_6]^{4-}$is oxidized resulting in the formation of the Fe(III) species ferricyanide ($[Fe(CN)_6]^{3-}$). Timescales and yield of the photo-oxidation have been initially established by time-resolved optical spectroscopies [1, 2, 3, 4]. However, in order to acquire information on the electronic structure and in particular valence orbital occupation core-level spectroscopies provide enhanced sensitivity.

With respect to the photo-oxidation of aqueous $[Fe(CN)_6]^{4-}$, time-resolved X-ray absorption spectroscopy at the Fe K-edge was used by Reinhard *et al.* to investigate the formation of $[Fe(CN)_6]^{3-}$from the metal perspective on a picosecond time-scale. Due to their quadrupole character, the analyzed pre-edge features are sensitive to the Fe 3d orbital occupation. This allowed Reinhard *et al.* to study the yield of photo-oxidation in the ultraviolet regime as well as competing relaxation pathways [5]. Complementary information from the ligand perspective can be acquired using time-resolved valence-to-core X-ray emission spectroscopy. March *et al.* used the technique to follow changes of the overlap between ligand and metal-centered orbitals for the case of the photo-oxidation of $[Fe(CN)_6]^{4-}$ [6].

In this work, we demonstrate how time-resolved X-ray absorption spectroscopy in the soft X-ray regime combines the capabilities of different spectroscopies in the hard X-ray regime by providing equivalent information regarding valence orbital occupation as seen from the metal as well as the ligand perspective. A liquid flatjet setup (see Materials and methods) is employed allowing for combined transmission experiments in the range of 3d metal L-edges [7] as well as K-edges of light elements [8]. This approach gives unique access to the unoccupied density of states locally at the Fe center through the Fe $2p \rightarrow 3d$ excitation of L-edge spectroscopy [9, 10, 11, 12, 13]. At the same time, information from the CN^- ligand perspective is given by the N $1s \rightarrow 2p$ excitation [14, 11, 15, 12, 16]. This allows to access equivalent valence orbitals using ligand- as well as metal-centered core-excitations, which provides experimental flexibility when targeting more complex systems. Furthermore, due to the transmission scheme of the experiment, quantitative absorption cross sections are recorded that allow to directly infer the number of photo-oxidized species as seen from the metal as well as the ligand perspective.

2. Results and discussion

In order to rationalize the soft X-ray signatures of the photo-induced interconversion of $[Fe(CN)_6]^{4-}$into its oxidized counterpart $[Fe(CN)_6]^{3-}$, we first introduce the steady-state features of the two species that have been analyzed previously [14, 17, 11]. Fig. 1 shows the X-ray absorption spectra of aqueous $[Fe(CN)_6]^{4-}$and $[Fe(CN)_6]^{3-}$measured at the N K-edge. The spectra are displayed as the measured absorbance A, which is retrieved by comparing the transmitted intensity I to the direct beam I_0 following Beer-Lambert's law:

$$A = -log_{10}\frac{I}{I_0} \quad (1)$$

Absorption from the solvent is subtracted assuming a

rajay@uni-potsdam.de (R.M. Jay)
ORCID(s): 0000-0001-9607-8264 (R.M. Jay); 0000-0002-1310-0735 (S. Eckert); 0000-0003-2689-8878 (M. Fondell); 0000-0003-4126-8233 (A. Föhlisch)
[1]Present address: Max Born Institute for Nonlinear Optics and Short Pulse Spectroscopy, Max-Born-Straße 2A, 12489 Berlin, Germany.

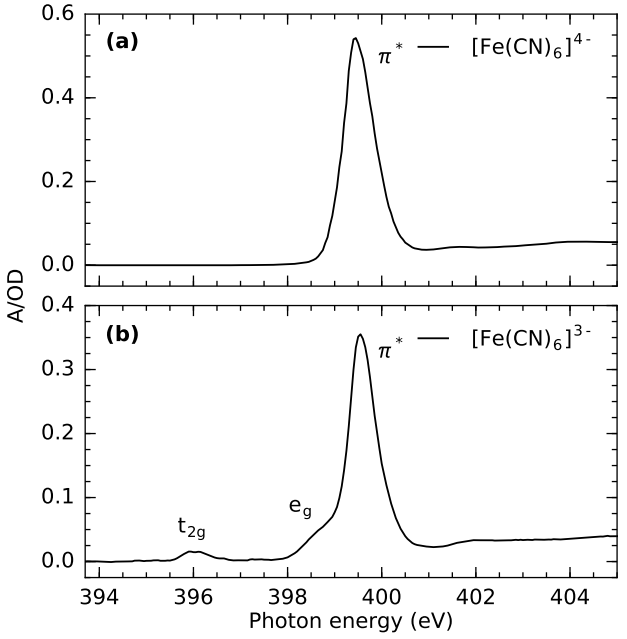

Figure 1: (a) N K-edge absorption spectrum of $[Fe(CN)_6]^{4-}$and **(b)** $[Fe(CN)_6]^{3-}$.

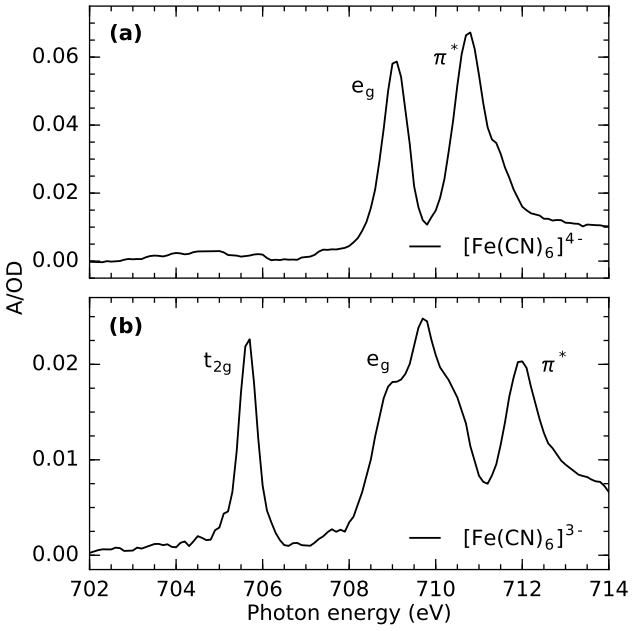

Figure 2: (a) Fe L_3-edge absorption spectrum of $[Fe(CN)_6]^{4-}$and **(b)** $[Fe(CN)_6]^{3-}$.

linear background determined from the slope before the absorption onset. For the N K-edge this amounts to ∼65% of the incident intensity, while ∼4% are absorbed by the solute (estimated from the absorbance at 405 eV). The spectrum of $[Fe(CN)_6]^{4-}$is displayed in Fig. 1a. The single intense absorption line can be attributed to the elevation of a N 1s electron into the unoccupied anti-bonding π^* system of the CN^- ligands [14, 11]. In the case of $[Fe(CN)_6]^{3-}$, its N K-edge absorption spectrum shown in Fig. 1b exhibits additional features. Due to the strong π-back-donation in these octahedral complexes, unoccupied ligand π^*-orbitals of t_{2g} symmetry can adapt some Fe 3d character. As the Fe(III) oxidation state of $[Fe(CN)_6]^{3-}$results in a t_{2g} hole, its spectrum exhibits a pre-edge resonance at 396 eV. This feature can consequently be attributed to a N 1s → Fe 3d(t_{2g}) transition [14, 11]. Similarly, the shoulder at 398.5 eV has previously been attributed to a N 1s → Fe 3d(e_g) excitation. This transition is expected to be present also in the case of $[Fe(CN)_6]^{4-}$, but, in this case, is argued to be obscured by the intense π^* resonance [11].

Similar orbital-specific assignments are applicable to the L_3-edge features of $[Fe(CN)_6]^{4-}$and $[Fe(CN)_6]^{3-}$, which are displayed in Fig. 2. Analogously to the N K-edge, the spectra are corrected for solvent absorption by subtracting a linear background. Here, ∼80% of the incident intensity is absorbed by the solvent, while less than 1% is absorbed by the solute (estimated from the absorbance at 714 eV). The spectrum of $[Fe(CN)_6]^{4-}$shown in Fig. 2a exhibits two intense resonances that have been assigned to be of Fe 2p → 3d(e_g) (709 eV) and Fe 2p → CN^- π^*(t_{2g}) character (710.8 eV) [17, 11]. For the case of $[Fe(CN)_6]^{3-}$shown in Fig. 2b, the two resonances at higher energies can be attributed to probe the same e_g (709.7 eV) and CN^- π^* (712 eV) orbitals as in the case of $[Fe(CN)_6]^{4-}$. Due to the hole in the t_{2g} orbital and the subsequent open-shell character of the species, multiplet-effects cause a broadening of the e_g resonance compared to $[Fe(CN)_6]^{4-}$in Fig. 2a [17, 11]. The reduced t_{2g} occupation also results in a lower intensity of the CN^- π^* resonance. The feature directly probes π-back-donation, an effect that has been shown to scale with t_{2g} occupation [17, 18, 19]. Lastly, and most importantly, an additional pre-edge feature arises at 705.6 eV due to the hole in the t_{2g} orbitals corresponding to a Fe 2p → 3d(t_{2g}) transition. The resonance therefore probes the same half-filled orbital as the pre-edge observed for the N K-edge of $[Fe(CN)_6]^{3-}$. This provides two independent fingerprints of the open-shell character of $[Fe(CN)_6]^{3-}$in the soft X-ray regime. It should be emphasized that, while the individual spectral features of $[Fe(CN)_6]^{3-}$and $[Fe(CN)_6]^{4-}$in the soft X-ray regime have been thoroughly investigated and assigned previously [14, 17, 11], the spectra presented here constitute, to the best of our knowledge, the first transmission measurements, which allow for the extraction of quantitative absorption cross sections of solution-phase $[Fe(CN)_6]^{3-}$and $[Fe(CN)_6]^{4-}$in the soft X-ray regime.

Having established the steady-state signatures of aqueous $[Fe(CN)_6]^{3-}$and $[Fe(CN)_6]^{4-}$, we move on to study their photo-induced interconversion. Fig. 3a and b show the N K-edge and Fe L_3-edge difference spectra between $[Fe(CN)_6]^{3-}$and $[Fe(CN)_6]^{4-}$from Fig. 1 and 2. While before, the spectra were displayed directly as the measured absorbance A, the difference spectra in Fig. 3a and b are displayed as changes of the extinction coefficient ϵ. This quantity can be calculated from the absorbance A by normalizing to the molar concentration c and thickness d of the sample (see Materials and Methods):

$$\epsilon = A/cd \quad (2)$$

Thereby, the extinction coefficient ϵ is retrieved as a quantity independent of experimental parameters allowing for a direct comparison of the steady-state spectra of $[Fe(CN)_6]^{3-}$and $[Fe(CN)_6]^{4-}$. Furthermore, the respective extinction coefficients compare well with transmission measurements on other Fe and N-containing transition metal complexes [10, 20].

We can therefore proceed to evaluate the transient difference spectra of $[Fe(CN)_6]^{4-}$measured at the N K-edge and Fe L_3-edge displayed in Fig. 3c and d, respectively. The transient spectra are retrieved by recording consecutive X-ray pulses transmitted through photo-excited and unexcited sample, respectively. The data is collected at a pump-probe delay of 80 ps with respect to the 257 nm laser excitation, where thermal effects are not anymore expected to influence the shape of the spectra [21, 22, 23]. Both spectra are normalized to the respective sample thickness d (see Materials and methods). The time-resolution of the experiment was (53 ± 8) ps as determined from the delay trace shown in the inset in Fig. 3c, which was recorded at 399.2 eV. The dynamics can be modeled by a step function which is broadened by the instrument response function. On the picosecond timescale investigated in this study and within the time-resolution of the experiment, the sample has therefore reached a meta-stable configuration. The general shape of the transient spectra on both edges resemble the steady-state difference spectra displayed in Fig. 3a and b. This can be expected from the photo-excitation of $[Fe(CN)_6]^{4-}$in the ultraviolet, where an electron is ejected into the solvent, thereby producing the oxidized $[Fe(CN)_6]^{3-}$.

Minor differences can, however, be observed due to competing photochemical channels. It has been shown that in the ultraviolet regime, a photo-aquation process can be triggered additionally, where a CN^- ligand is detached and replaced by a water molecule [24, 5, 25]. At the N K-edge shown in Fig. 3c, the free CN^- ligand as well as the photo-aquated complex $[Fe(CN)_5(H_2O)]^{3-}$ can therefore be expected to cause the higher intensities at 398.6 eV and 399.7 eV relative to the t_{2g} intensity at 396 eV when compared to the steady-state difference in Fig. 3a. To substantiate this assignment, we performed spectrum simulations (see Materials and methods) based on time-dependent density functional theory (TD-DFT) for $[Fe(CN)_6]^{4-}$, $[Fe(CN)_6]^{3-}$, $[Fe(CN)_5(H_2O)]^{3-}$ as well as the CN^- group. The results for the N K-edge are displayed in Fig. 3e. It can be clearly seen that both, the photo-aquated complex as well as the CN^- group, can be expected to contribute to the enhanced intensity at 398.6 eV with respect to the steady-state difference. Furthermore, the main resonance of $[Fe(CN)_5(H_2O)]^{3-}$ exhibits a slight shift to higher energies, therefore also providing an explanation for the higher intensity at 399.7 eV.

Similarly, at the L_3-edge, additional intensity can be observed at 708.4 eV in the transient spectrum (compare Fig. 3d) which is absent in the steady-state difference spectrum in Fig. 3c. Assuming again the presence of the photo-aquated species, this intensity could be caused by the reduced symmetry of the species, where the resulting Jahn-Teller distortion would be expected to split the e_g levels. As for the N K-edge, this is verified by our TD-DFT calculations displayed in Fig. 3e. $[Fe(CN)_5(H_2O)]^{3-}$ indeed shows intensity below the absorption onset of $[Fe(CN)_6]^{4-}$, thereby giving a reasonable explanation for the feature at 708.4 eV. It should be noted that Reinhard et al. [5] suggested that the additional spectral features not arising from the photo-oxidation channel were also caused by a re-excitation of the already oxidized product due to their long laser pump pulses. The laser pulse lengths applied in this work are much closer to the previously reported femtosecond timescale of photo-oxidation [3] (see Materials and methods), which can be expected to reduce the likeliness of a consecutive laser excitation. In conjunction with the good agreement with the spectrum simulations, a re-excitation of the photo-oxidized species is therefore tentatively ruled out in our case.

Despite the detection of the photo-aquated species, the opening of the t_{2g} resonance in both absorption edges as the result of the photo-excitation could be established as clear signatures of changes in valence orbital occupation and thus, the creation of $[Fe(CN)_6]^{3-}$. We can therefore move on to quantitatively determine the fraction of photo-oxidized molecules detected in the experiment. As outlined previously, the pre-edge resonances due to core-to-t_{2g} excitation arising at both edges in the case of the open-shell $[Fe(CN)_6]^{3-}$can serve as unambiguous fingerprints of oxidation recorded in background-free regions of the spectra. The two pre-edge regions at the N K-edge and Fe L_3-edge are also not expected to exhibit contributions from precursors to the oxidized species since the photo-oxidation has been shown to be complete on a femtosecond timescale [3]. Similarly, contributions by precursors of the competing photochemical pathway can be excluded, as the photo-aquation process involves only closed-shell species on the picosecond timescale studied here [25].

It is important to note that the steady-state difference spectra in Fig. 3a and b constitute the absolute difference of the respective extinction coefficients ϵ, while the transient spectra in Fig. 3c and d on the other hand are normalized only to the sample thickness d. The concentration of transient molecules c can therefore be used to retrieve the absolute number of photo-oxidized species in the transient difference spectrum. This is done by modeling the pre-edge features at 396 eV and 705.6 eV in the steady-state as well as time-resolved difference spectra by gaussian functions. The deduced peak intensities from the steady-state differences are then used to scale the time-resolved difference spectra by the concentration c, which yields the number of photo-oxidized molecules. This results in (3.1 ± 0.6) mM photo-oxidized species at the N K-edge and (3.7 ± 0.9) mM at the Fe L_3-edge. The corresponding errors are due to uncertainties in the sample thickness as well as the statistical error resulting from the fitting procedure. Absolute errors in the measurement of the diode current as a measure of the ab-

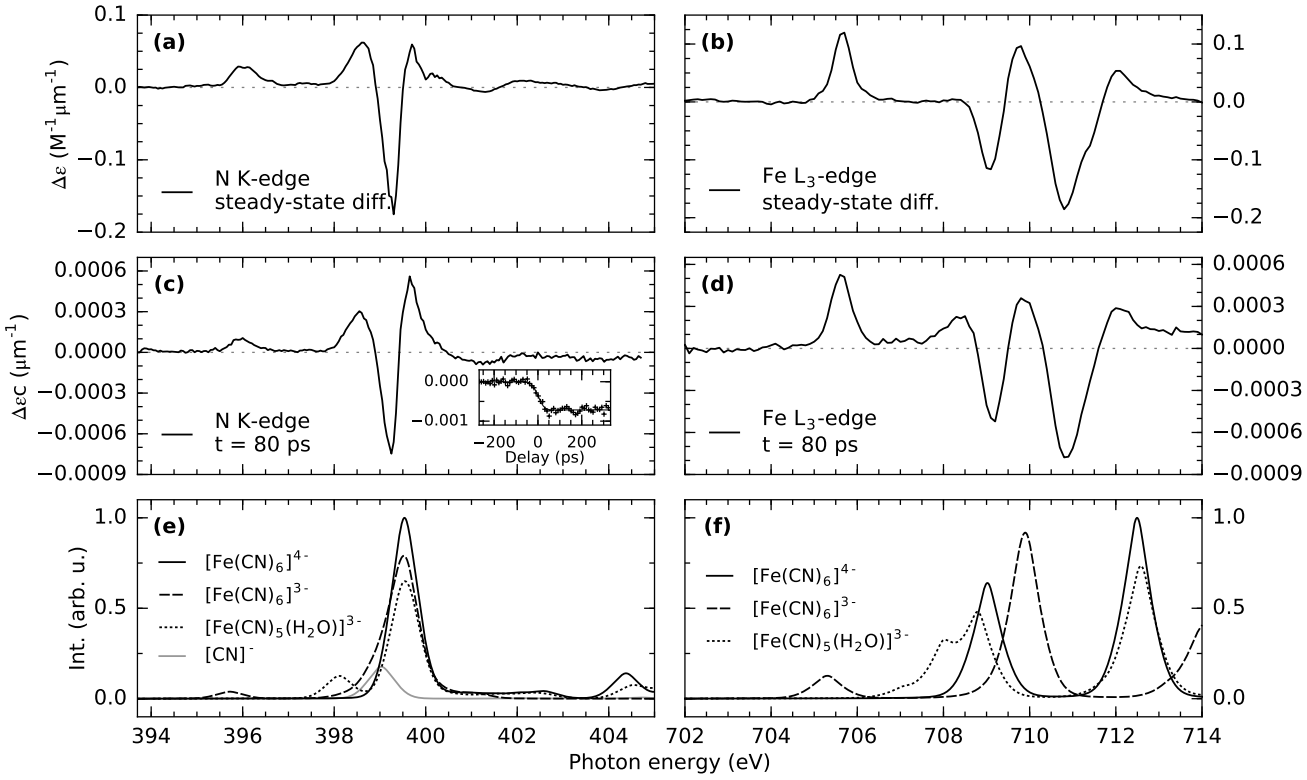

Figure 3: **(a)** X-ray absorption difference spectrum between the steady-state spectra of $[Fe(CN)_6]^{3-}$and $[Fe(CN)_6]^{4-}$for the N K-edge from Fig. 1 and **(b)** Fe L_3-edge from Fig. 2. **(c)** Transient absorption difference spectrum of $[Fe(CN)_6]^{4-}$after photo-excitation for the N K-edge. The inset shows a delay trace measured at 399.2 eV. **(d)** Transient absorption difference spectrum of $[Fe(CN)_6]^{4-}$measured at the Fe L_3-edge.**(e)** Spectrum simulations based on TD-DFT for the N K-edge and **(f)** Fe L_3-edge.

sorption signal (see Materials and methods) are on the order of 10^{-4} and are therefore neglected. It should be emphasized that the good agreement between the two independent measurements demonstrates the robustness of the underlying core-excitations as two independent measures of the Fe 3d occupation not only on a qualitative but also quantitative level. This provides experimental flexibility to measurements in the soft X-ray regime that can be beneficial when following the photochemistry of 3d transition metal complexes.

3. Conclusion

In summary, we have presented first quantitative solution-phase soft X-ray transmission data on aqueous $[Fe(CN)_6]^{4-}$and $[Fe(CN)_6]^{3-}$. The photochemistry of $[Fe(CN)_6]^{4-}$following a 257 nm photo-excitation was investigated using time-resolved X-ray absorption spectroscopy at the N K-edge as well as Fe L_3-edge. Thereby, signatures of photo-oxidation of $[Fe(CN)_6]^{4-}$were detected and used to independently evaluate the number of oxidized molecules from the ligand as well as metal perspective. Our study thus exemplifies the selectivity of time-resolved soft X-ray absorption spectroscopy to the valence orbital occupation of photo-excited 3d transition metal complexes. In particular, it was shown how the technique provides unique flexibility since equivalent information can be extracted from ligand- as well as metal-centric absorption measurements which are both accessible in the soft X-ray range.

4. Materials and methods

$K_4Fe(CN)_6{\cdot}(H_2O)_3$ and $K_3Fe(CN)_6$ were purchased from Sigma-Aldrich and used without further purification. Samples were prepared as 150 mM solutions in deionized water for the case of $[Fe(CN)_6]^{4-}$, while for the measurements of $[Fe(CN)_6]^{3-}$, 100 mM solutions were used.

The experimental data was measured at the UE52-SGM beamline [26] of the BESSY II synchrotron using a setup dedicated to soft X-ray absorption measurements in transmission mode. Details of the experimental setup can be found elsewhere [27]. Preparatory and complementary measurements were conducted at EDAX@UE49-SGM. The employed liquid flatjet system provided liquid sample sheets of (5.6 ± 0.6) μm thickness at the N K-edge and (1.8 ± 0.3) μm at the Fe L_3-edge as determined from the solvent absorption before the absorption onset in comparison to tabulated values [28]. The associated error is estimated from deviations between individual scans measured at the respective absorption edges. The flow speed of the sample was between 1.8 ml/min and 1.9 ml/min throughout all measurements. The resulting rate of sample replenishment has been

shown to be sufficient to avoid X-ray-induced sample damage [29]. The X-ray intensity transmitted through the sample is detected by an GaAs photodiode for the steady-state measurements. An avalanche photodiode is used for the time-resolved measurements. The full X-ray fluence of the beamline was 5×10^{10} photons/s at both absorption edges at a spot size of $60 \times 120\ \mu m^2$. The bandwidth of the incoming radiation was 0.13 eV at 390 eV and 0.2 eV at 700 eV. The sample was excited using laser pulses at a central wavelength of 257 nm and roughly 300 fs pulse length. At a laser spot size of $50 \times 50\ \mu m^2$, an excitation density of $100\ mJ/cm^2$ is provided. Estimated from the extinction coefficient of $[Fe(CN)_6]^{4-}$ at 257 nm [5] and the presented experimental parameters, 38% of the incoming laser intensity is absorbed in the measurements at the N K-edge and 14% at the Fe L-edge. The laser was operated at a repetition rate of 208 kHz allowing the sample to be fully replenished (within $>2\ \mu s$) between individual pump pulses as well as before the unpumped reference measurement. About 1% of the comparably high laser excitation density is estimated to contribute to the two-photon ionization of water [30]. This results in additional solvated electrons at a ratio of about $1{:}10^4$ compared to the number of bulk water molecules. Since electrons generated by water photolysis have additionally been shown to recombine on timescales below the time-resolution [31], a contamination of the spectra can be safely excluded.

DFT calculations were performed on the B3LYP level [32, 33] using the Orca quantum chemistry package [34]. The def2-TZVP(-f) basis set [35] as well as the RIJCOSX method [34] with the def2-TZV/J auxiliary basis set [36] were employed throughout all calculations. The water solvent was modeled using the COSMO method [37]. The Becke-Johnson damping scheme was utilized for dispersion correction [38, 39]. All spectra were calculated using TD-DFT. To match the experimental data, a Lorentzian broadening of 0.13 eV [40] and a Gaussian broadening of 0.65 eV was applied to the calculated transitions of the N K-edge. The spectra were then shifted by 12 eV. Similarly, for the Fe L_3-edge, a Lorentzian broadening of 0.4 eV [40] and a Gaussian broadening of 0.7 eV was applied. The spectra were then shifted by 9 eV for agreement with the experiment.

Acknowledgments

R.M.J., S.E. and A.F. acknowledge funding from the ERC-ADG-2014 - Advanced Investigator Grant No. 669531 EDAX under the Horizon 2020 EU Framework Program for Research and Innovation. We thank the Helmholtz-Zentrum Berlin for allocation of synchrotron radiation beamtime and Christian Weniger for technical support during the measurements. We thank Vinícius Vaz da Cruz for fruitful discussions about the quantum chemical simulations.

References

[1] M. Shirom, G. Stein, Excited State Chemistry of the Ferrocyanide Ion in Aqueous Solution. I. Formation of the Hydrated Electron, The Journal of Chemical Physics 55 (1971) 3372–3378.

[2] J. C. Mialocq, J. Sutton, P. Goujon, Picosecond study of photoionization in aqueous solution, Il Nuovo Cimento B Series 11 63 (1981) 317–321.

[3] S. Pommeret, R. Naskrecki, P. van der Meulen, M. Ménard, G. Vigneron, T. Gustavsson, Ultrafast events in the electron photodetachment from the hexacyanoferrate(II) complex in solution, Chemical Physics Letters 288 (1998) 833–840.

[4] N. A. Anderson, K. Hang, J. B. Asbury, T. Lian, Ultrafast mid-IR detection of the direct precursor to the presolvated electron following electron ejection from ferrocyanide, Chemical Physics Letters 329 (2000) 386–392.

[5] M. Reinhard, T. J. Penfold, F. A. Lima, J. Rittmann, M. H. Rittmann-Frank, R. Abela, I. Tavernelli, U. Rothlisberger, C. J. Milne, M. Chergui, Photooxidation and photoaquation of iron hexacyanide in aqueous solution: A picosecond X-ray absorption study, Structural Dynamics 1 (2014) 0–12.

[6] A. M. March, T. A. Assefa, C. Bressler, G. Doumy, A. Galler, W. Gawelda, E. P. Kanter, Z. Németh, M. Pápai, S. H. Southworth, L. Young, G. Vankó, Feasibility of Valence-to-Core X-ray Emission Spectroscopy for Tracking Transient Species, The Journal of Physical Chemistry C 119 (2015) 14571–14578.

[7] M. Kubin, M. Guo, M. Ekimova, M. L. Baker, T. Kroll, E. Källman, J. Kern, V. K. Yachandra, J. Yano, E. T. J. Nibbering, M. Lundberg, P. Wernet, Direct Determination of Absolute Absorption Cross Sections at the L-Edge of Dilute Mn Complexes in Solution Using a Transmission Flatjet, Inorganic Chemistry 57 (2018) 5449–5462.

[8] M. Ekimova, W. Quevedo, M. Faubel, P. Wernet, E. T. J. Nibbering, A liquid flatjet system for solution phase soft-x-ray spectroscopy, Structural Dynamics 2 (2015) 054301.

[9] E. C. Wasinger, F. M. F. de Groot, B. Hedman, K. O. Hodgson, E. I. Solomon, L-edge X-ray Absorption Spectroscopy of Non-Heme Iron Sites: Experimental Determination of Differential Orbital Covalency, Journal of the American Chemical Society 125 (2003) 12894–12906.

[10] N. Huse, T. K. Kim, L. Jamula, J. K. McCusker, F. M. F. de Groot, R. W. Schoenlein, Photo-Induced Spin-State Conversion in Solvated Transition Metal Complexes Probed via Time-Resolved Soft X-ray Spectroscopy, Journal of the American Chemical Society 132 (2010) 6809–6816.

[11] K. Kunnus, W. Zhang, M. G. Delcey, R. V. Pinjari, P. S. Miedema, S. Schreck, W. Quevedo, H. Schröder, A. Föhlisch, K. J. Gaffney, M. Lundberg, M. Odelius, P. Wernet, Viewing the Valence Electronic Structure of Ferric and Ferrous Hexacyanide in Solution from the Fe and Cyanide Perspectives, The Journal of Physical Chemistry B 120 (2016) 7182–7194.

[12] R. M. Jay, S. Eckert, M. Fondell, P. S. Miedema, J. Norell, A. Pietzsch, W. Quevedo, J. Niskanen, K. Kunnus, A. Föhlisch, The nature of frontier orbitals under systematic ligand exchange in (pseudo-)octahedral Fe(II) complexes, Physical Chemistry Chemical Physics 20 (2018) 27745–27751.

[13] R. M. Jay, S. Eckert, V. Vaz da Cruz, M. Fondell, R. Mitzner, A. Föhlisch, Covalency-Driven Preservation of Local Charge Densities in a Metal-to-Ligand Charge-Transfer Excited Iron Photosensitizer, Angewandte Chemie International Edition 58 (2019) 10742–10746.

[14] A. Vinogradov, A. Preobrajenski, A. Knop-Gericke, S. Molodtsov, S. Krasnikov, S. Nekipelov, R. Szargan, M. Hävecker, R. Schlögl, Observation of back-donation in 3d metal cyanide complexes through N K absorption spectra, Journal of Electron Spectroscopy and Related Phenomena 114-116 (2001) 813–818.

[15] S. Eckert, J. Niskanen, R. M. Jay, P. S. Miedema, M. Fondell, B. Kennedy, W. Quevedo, M. Iannuzzi, A. Föhlisch, Valence orbitals and local bond dynamics around N atoms of histidine under X-ray irradiation, Physical Chemistry Chemical Physics 19 (2017) 32091–32098.

[16] S. Eckert, J. Norell, R. M. Jay, M. Fondell, R. Mitzner, M. Odelius, A. Föhlisch, T_1 Population as the Driver of Excited-State Proton-Transfer in 2-Thiopyridone, Chemistry - A European Journal 25 (2019) 1733–1739.

[17] R. K. Hocking, E. C. Wasinger, F. M. F. de Groot, K. O. Hodgson,

B. Hedman, E. I. Solomon, Fe L-Edge XAS Studies of $K_4[Fe(CN)_6]$ and $K_3[Fe(CN)_6]$: A Direct Probe of Back-Bonding, Journal of the American Chemical Society 128 (2006) 10442–10451.

[18] R. M. Jay, J. Norell, S. Eckert, M. Hantschmann, M. Beye, B. Kennedy, W. Quevedo, W. F. Schlotter, G. L. Dakovski, M. P. Minitti, M. C. Hoffmann, A. Mitra, S. P. Moeller, D. Nordlund, W. Zhang, H. W. Liang, K. Kunnus, K. Kubiček, S. A. Techert, M. Lundberg, P. Wernet, K. Gaffney, M. Odelius, A. Föhlisch, Disentangling Transient Charge Density and Metal-Ligand Covalency in Photoexcited Ferricyanide with Femtosecond Resonant Inelastic Soft X-ray Scattering, The Journal of Physical Chemistry Letters 9 (2018) 3538–3543.

[19] L. H. Jones, Nature of Bonding in Metal Cyanide Complexes as Related to Intensity and Frequency of Infrared Absorption Spectra, Inorganic Chemistry 2 (1963) 777–780.

[20] B. E. Van Kuiken, H. Cho, K. Hong, M. Khalil, R. W. Schoenlein, T. K. Kim, N. Huse, Time-Resolved X-ray Spectroscopy in the Water Window: Elucidating Transient Valence Charge Distributions in an Aqueous Fe(II) Complex, Journal of Physical Chemistry Letters 7 (2016) 465–470.

[21] S. E. Canton, K. S. Kjær, G. Vankó, T. B. van Driel, S.-i. Adachi, A. Bordage, C. Bressler, P. Chabera, M. Christensen, A. O. Dohn, A. Galler, W. Gawelda, D. Gosztola, K. Haldrup, T. Harlang, Y. Liu, K. B. Møller, Z. Németh, S. Nozawa, M. Pápai, T. Sato, T. Sato, K. Suarez-Alcantara, T. Togashi, K. Tono, J. Uhlig, D. A. Vithanage, K. Wärnmark, M. Yabashi, J. Zhang, V. Sundström, M. M. Nielsen, Visualizing the non-equilibrium dynamics of photoinduced intramolecular electron transfer with femtosecond X-ray pulses, Nature Communications 6 (2015) 6359.

[22] J. Ojeda, C. A. Arrell, L. Longetti, M. Chergui, J. Helbing, Charge-transfer and impulsive electronic-to- vibrational energy conversion in ferricyanide: ultrafast photoelectron and transient infrared studies, Phys. Chem. Chem. Phys. 19 (2017) 17052–17062.

[23] K. Kunnus, M. Vacher, T. C. B. Harlang, K. S. Kjær, K. Haldrup, E. Biasin, T. B. van Driel, M. Pápai, P. Chabera, Y. Liu, H. Tatsuno, C. Timm, E. Källman, M. Delcey, R. W. Hartsock, M. E. Reinhard, S. Koroidov, M. G. Laursen, F. B. Hansen, P. Vester, M. Christensen, L. Sandberg, Z. Németh, D. S. Szemes, É. Bajnóczi, R. Alonso-Mori, J. M. Glownia, S. Nelson, M. Sikorski, D. Sokaras, H. T. Lemke, S. E. Canton, K. B. Møller, M. M. Nielsen, G. Vankó, K. Wärnmark, V. Sundström, P. Persson, M. Lundberg, J. Uhlig, K. J. Gaffney, Vibrational wavepacket dynamics in Fe carbene photosensitizer determined with femtosecond X-ray emission and scattering, Nature Communications 11 (2020) 634.

[24] M. Shirom, G. Stein, Excited State Chemistry of the Ferrocyanide Ion in Aqueous Solution. II. Photoaquation, The Journal of Chemical Physics 55 (1971) 3379–3382.

[25] M. Reinhard, G. Auböck, N. A. Besley, I. P. Clark, G. M. Greetham, M. W. D. Hanson-Heine, R. Horvath, T. S. Murphy, T. J. Penfold, M. Towrie, M. W. George, M. Chergui, Photoaquation Mechanism of Hexacyanoferrate(II) Ions: Ultrafast 2D UV and Transient Visible and IR Spectroscopies, Journal of the American Chemical Society 139 (2017) 7335–7347.

[26] P. S. Miedema, W. Quevedo, M. Fondell, The variable polarization undulator beamline UE52 SGM at BESSY II, Journal of large-scale research facilities JLSRF 2 (2016) A70.

[27] M. Fondell, S. Eckert, R. M. Jay, C. Weniger, W. Quevedo, J. Niskanen, B. Kennedy, F. Sorgenfrei, D. Schick, E. Giangrisostomi, R. Ovsyannikov, K. Adamczyk, N. Huse, P. Wernet, R. Mitzner, A. Föhlisch, Time-resolved soft X-ray absorption spectroscopy in transmission mode on liquids at MHz repetition rates, Structural Dynamics 4 (2017) 054902.

[28] B. Henke, E. Gullikson, J. Davis, X-Ray Interactions: Photoabsorption, Scattering, Transmission, and Reflection at E = 50-30,000 eV, Z = 1-92, Atomic Data and Nuclear Data Tables 54 (1993) 181–342.

[29] M. Kubin, J. Kern, M. Guo, E. Källman, R. Mitzner, V. K. Yachandra, M. Lundberg, J. Yano, P. Wernet, X-ray-induced sample damage at the Mn L-edge: a case study for soft X-ray spectroscopy of transition metal complexes in solution, Physical Chemistry Chemical Physics 20 (2018) 16817–16827.

[30] D. N. Nikogosyan, A. A. Oraevsky, V. I. Rupasov, Two-photon ionization and dissociation of liquid water by powerful laser UV radiation, Chemical Physics 77 (1983) 131–143.

[31] Z. Loh, G. Doumy, C. Arnold, L. Kjellsson, S. H. Southworth, A. A. Haddad, Y. Kumagai, M. Tu, P. J. Ho, A. M. March, R. D. Schaller, M. S. B. M. Yusof, T. Debnath, M. Simon, R. Welsch, L. Inhester, K. Khalili, K. Nanda, A. I. Krylov, S. Moeller, G. Coslovich, J. Koralek, M. P. Minitti, W. F. Schlotter, Observation of the fastest chemical processes in the radiolysis of water, Science 367 (2020) 179–182.

[32] A. D. Becke, Density-functional exchange-energy approximation with correct asymptotic behavior, Phys. Rev. A 38 (1988) 3098–3100.

[33] A. D. Becke, A new mixing of hartree-fock and local density-functional theories, The Journal of Chemical Physics 98 (1993) 1372–1377.

[34] F. Neese, The orca program system, Wiley Interdisciplinary Reviews: Computational Molecular Science 2 (2012) 73–78.

[35] F. Weigend, R. Ahlrichs, Balanced basis sets of split valence, triple zeta valence and quadruple zeta valence quality for h to rn: Design and assessment of accuracy, Phys. Chem. Chem. Phys. 7 (2005) 3297–3305.

[36] F. Weigend, Accurate coulomb-fitting basis sets for h to rn, Phys. Chem. Chem. Phys. 8 (2006) 1057–1065.

[37] A. Klamt, G. Schuurmann, Cosmo: a new approach to dielectric screening in solvents with explicit expressions for the screening energy and its gradient, J. Chem. Soc., Perkin Trans. 2 (1993) 799–805.

[38] S. Grimme, J. Antony, S. Ehrlich, H. Krieg, A consistent and accurate ab initio parametrization of density functional dispersion correction (dft-d) for the 94 elements h-pu, The Journal of Chemical Physics 132 (2010) 154104.

[39] S. Grimme, S. Ehrlich, L. Goerigk, Effect of the damping function in dispersion corrected density functional theory, Journal of Computational Chemistry 32 (2011) 1456–1465.

[40] J. Campbell, T. Papp, Widths of the atomic K-N7 levels, Atomic Data and Nuclear Data Tables 77 (2001) 1–56.